Analysis of the Sound Field Characteristics of a Muffler at Different Flow Conditions

J. W. Lin[1], H. L. Liu[1], L. Dong[1†], R. Z. Zhou[1] and R. N. Hua[2]

[1] *Research Center of Fluid Machinery Engineering and Technology, Jiangsu University, Zhenjiang 212013, China*
[2] *Wuhan Second Ship Design and Research Institute, Wuhan, 430060, China*

†*Corresponding Author Email: dongliang@ujs.edu.cn*

ABSTRACT

To reduce the noise in a pump piping system and increase the usage time of equipment, a new type of porous muffler is proposed in this paper. A water guide cone is incorporated into the muffler structure, which may help to redirect the fluid media in the piping system. The porous structure is adapted from a muffler shell, water cone wall and round bottom plate. According to this structure, the muffler sample is made, and a pump pipeline system test bench is set up. The outlet noise of the pump pipeline system is measured after installing the muffler. At the same time, the muffler is numerically simulated by combining computational fluid mechanics and Lighthill acoustic theory. The characteristics of the flow field and external sound field under three different flow conditions of 200 m^3/h, 400 m^3/h and 600 m^3/h are assessed. The numerical simulation results show the same dominant frequency and trend as the experimental results. The rationality of the numerical simulation is verified. Research shows that: the level of sound pressure at the muffler's outlet is lower than at the inlet, causing muffling, and the characteristics of a quadrupole sound source appear at the outlet. The proposed muffler has a certain effect in reducing noise in the pump pipeline system.

NOMENCLATURE

G_k	generating term for the turbulent kinetic energy	ζ	flow resistance coefficient
σ_k	Prandtl numbers of turbulent kinetic energy	ρ	media density
σ_ε	Prandtl numbers of dissipation rate	v	average flow
T_{ij}	Lighthill stress tensor	k	turbulent kinetic energy
ε	dissipation rate	Δp	pressure loss
SPL	Sound Pressure Level	$OASPL$	Overall pressure level
N-S	Navier-Stokes	C_0	value of the sound velocity
P	pressure	t	time
μ	coefficient of viscosity	g	acceleration of gravity

1. INTRODUCTION

Mufflers are widely used in the ocean engineering, aerospace, and power industries and other fields that require pump pipeline system. Whether for civilian or military applications, the demand for muted noise reduction is increasing. The vibration and noise problems of high power pipeline systems have becoming increasingly prominent. The vibration and noise of a pumping pipeline system are mainly produced by pump group vibrations and fluid excitations in the pipeline. The appearance of noise has adverse factors, such as affecting the service life of equipment, damaging human health and affecting the stealth performance of ships (Liang 2010; Liu *et al.* 2013; Dai *et al.* 2021). Noise can be eliminated effectively, and negative factors can be avoided by the design and installation of silencer equipment in pump pipeline systems (Gu *et al.* 2018).

Acoustic wave propagation and acoustic transmission in metamaterial pipeline systems with Helmholtz resonators were studied by Li *et al.* (2016). Bandgaps could be generated by the

introduction of periodic Helmholtz resonators in a pipeline system. Thus, the bandwidth and attenuation effect of the Helmholtz resonator were improved significantly. In some special cases, Bragg clearance interacted with resonant clearance to produce ultrawide coupling clearance. The explicit formula of precise bandgap coupling was extracted, and some key parameters of coupling gap width modulation and attenuation coefficient were studied. The coupling gap could be located in any frequency range, making low-frequency noise control feasible over the broadband range. A low-noise pipe drainage device was proposed by Xia *et al.* (2017). The device suppressed pressure pulsation mainly through an accumulator group and Helmholtz resonator. Noise reduction was achieved by suppressing the pressure pulsation at the pump outlet in the pipeline system. A Helmholtz resonance muffler was designed by Lyu *et al.* (2020). The structural parameters of the muffler were optimized by a genetic algorithm and numerical calculations were carried out. Finally, the frequency band of the muffler was expanded from 32 Hz to 86 Hz. All the mufflers mentioned above were based on Helmholtz resonance. Although a Helmholtz resonance muffler has a high low-frequency noise attenuation, its noise attenuation band is very narrow and has limitations. It can only mute at resonant frequencies. When deviating from the resonance frequency, the noise attenuation effect is not particularly obvious. Therefore, this kind of muffler is difficult to apply in practical situations where the excitation frequency changes or the muffler frequency band is wide (Shao *et al.* 2020; Zhang *et al.* 2021; Chen *et al.* 2017).

A muffler design method based on topology optimization was proposed, and experimental verification was carried out by Lee (2015). Using acoustic topology optimization, a partition volume minimization problem was proposed to achieve transmission loss. The muffler design problems at several target frequencies were solved, and the influence of the initial design variables on the optimal topology was studied. An expansion cavity muffler structure with a periodically arranged microperforated panel was proposed by Gai *et al.* (2020). The transfer matrix method and finite element method were used to analyze the transmission loss of the expansion cavity before and after the introduction of the microperforated plate. The sound insulation performance of the expansion cavity was further improved by adding a double-layer microperforated plate. To improve the performance of plate mufflers, Hou *et al.* (2020) focused on the study of plate mufflers. A plate muffler model with an elastic back cavity structure was proposed. The influence of the elastic back plate's structural parameters and the muffler noise mechanism were investigated and compared to the rigid back cavity model that is currently in use. A new multicavity perforated muffler structure was proposed by Zhou *et al.* (2018). The effect of the perforated cavity spacing on performance was studied. A genetic algorithm was used to optimize the sound of the muffler. The noise transmission characteristics of mufflers were studied by Xiang *et al.* (2017). A multicavity microperforated muffler

with adjustable transfer loss was proposed. The experimental results showed that the middle and low-frequency noise could be simultaneously suppressed by the muffler. The influence of baffles on the acoustic characteristics of microperforated tube mufflers was analyzed by Zuo *et al.* (2014). It was found that the position of the baffle affects the main acoustic attenuation band and transmission loss. The closer the baffle was to the middle position, the higher the frequency of the first arch attenuation domain, and the greater the transfer loss. The transfer loss increased when the number of partitions increased. However, when the number of partitions reached a certain value, the transfer loss did not increase significantly. Although the muffler could achieve the effect of noise reduction, the structure was more complex, technologically advanced, and difficult to process. The muffling effects were improved only in the medium and high-frequency ranges, and had certain limitations. This paper proposes a new type of muffler with a simple structure that is simple to process and install. The muffler has a very wide muffling frequency band and can simultaneously reduce low-frequency, mid-frequency and high-frequency noise at the outlet of the pump piping system, which has a wider application range and exceeds the limitations of the previous mufflers.

2. MUFFLER STRUCTURE and TEST PROGRAM

This paper presents a porous silencer for a pump piping system. The muffler at the pump line system's outlet muffles the sound. The muffler is primarily made up of two parts. The first part is the shell part of the muffler. The second part is the internal water guide cone, which is supported and fixed by three water guide cones. The shell and water cone surfaces contain a large number of round holes. The internal water cone redirects the fluid as it passes through the muffler. The conical shape and top arc design of the water guiding cone can reduce noise caused by fluid impact in the transition structure of different sections. They can effectively reduce vibration and noise. The muffler shell, the water guide cone's wall surface, and the round bottom plate has a huge number of circular holes that are all uniformly spaced. The muffler shell has three times the flow area of the water guide cone. The structure utilizes the high acoustic impedance of the pores to achieve noise reduction for the pump piping system. The structural diagram of the muffler is shown in Fig. 1.

The muffler samples are made, and a test bench is erected in accordance with the muffler structure scheme obtained above. The sample muffler is shown in Fig. 2. It is linked to the pump piping system's outlet. It is installed and secured in the water. The testing system is depicted in Fig. 3. The test device consists of a booster pump, valve, pressure transmitter, motor, flowmeter, muffler, and data acquisition system. Data acquisition equipment mainly collects high-frequency signals and low-frequency signals at the same time. Hydrophones are fitted at the muffler's inlet and outlet sites to measure
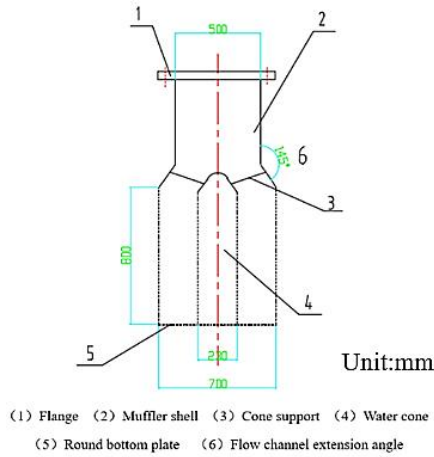
Fig. 1. Structure diagram of the muffler.

(1) Flange　(2) Muffler shell　(3) Cone support　(4) Water cone

(5) Round bottom plate　(6) Flow channel extension angle
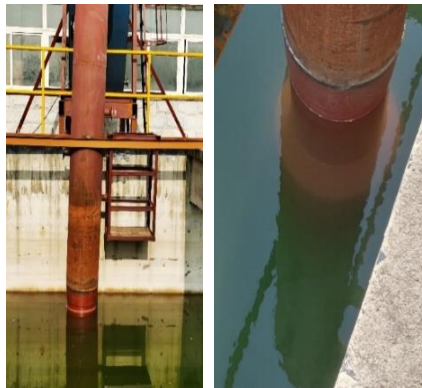

Fig. 2. Muffler Sample.

Fig. 3. Pump pipeline test system.

noise. The RHSA-20 hydrophone model is used throughout the test. The sensitivity of this hydrophone is 1.92 mV/Pa. The hardware conversion of the acquisition template inputs the sensor's output signal into the virtual instrument driver when the pump is operating. The noise signal is displayed and acquired using LabVIEW software. The instruments for signal acquisition are depicted in Fig. 4. The sampling interval of the acquisition module and the number of samples are determined using the Nyquist sampling theorem and the test range of noise (Liu *et al*. 2022). In general, the sampling frequency of the highest useful frequency is repeated three to four times. The frequency of

Fig. 4. Data collector.

sampling is determined to be 10240 Hz. The number of samples is determined to be N=30720.

3. NUMERICAL SIMULATION METHODS

3.1 Numerical Simulation Theory

Numerical simulation theory of the flow field

Because the pressure change inside the muffler is small, it can be classified as turbulent incompressible fluid flow. The whole process can be described by control equations such as the continuity equation, Reynolds mean N-S equation (Navier-Stokes equation), turbulent kinetic energy k, and transport equation for the turbulent kinetic energy dissipation rate ε (Zhang *et al*. 2006):

$$\frac{\partial u}{\partial x} + \frac{\partial v}{\partial y} + \frac{\partial w}{\partial z} = 0 \tag{1}$$

$$\rho \left(\frac{\partial w}{\partial t} + u\frac{\partial w}{\partial x} + v\frac{\partial w}{\partial y} + w\frac{\partial w}{\partial z} \right) = \frac{-\partial p}{\partial z}$$
$$+ \mu \left(\frac{\partial^2 w}{\partial x^2} + \frac{\partial^2 w}{\partial y^2} + \frac{\partial^2 w}{\partial z^2} \right) - \rho g \tag{2}$$

Where ρ is the density. P is the pressure. u, v and w are the components of the velocity vector in the x, y and z directions. t is the time. μ is the coefficient of viscosity and g is the acceleration of gravity.

$$\frac{\partial k}{\partial t} + u_j \frac{\partial k}{\partial x_j} = \frac{\partial}{\partial x_j}\left[\left(v + \frac{v_t}{\sigma_k}\right)\frac{\partial k}{\partial x_j}\right] + G_k - \varepsilon \tag{3}$$

$$\frac{\partial \varepsilon}{\partial t} + u_j \frac{\partial k}{\partial x_j} = \frac{\partial}{\partial x_j}\left[\left(v + \frac{v_t}{\sigma_\varepsilon}\right)\frac{\partial \varepsilon}{\partial x_j}\right] + C_{\varepsilon 1}\frac{\varepsilon}{k}G_k C_{\varepsilon 2}\frac{\varepsilon^2}{k} \tag{4}$$

$$v_t = C_\mu \frac{k^2}{\varepsilon} \tag{5}$$

where G_k is the generating term for the turbulent kinetic energy k due to the mean velocity gradient. σ_k and σ_ε are the Prandtl numbers of turbulent kinetic energy k and dissipation rate ε, respectively. $C_{\varepsilon 1}$, $C_{\varepsilon 2}$ and C_μ are empirical constants and are usually taken as $C_{\varepsilon 1}$=1.44，$C_{\varepsilon 2}$=1.92，C_μ=0.09.

The flow resistance coefficient ξ is used to express the resistance of the muffler to the passing medium. A larger value indicates a poorer flow capacity of the

muffler. The equation for calculating the flow resistance coefficient ξ is shown in Eq. (6). (Lighthill 1954; Liu *et al.* 2020):

$$\xi = \frac{\Delta p}{\left(\frac{\rho v^2}{2}\right)} \qquad (6)$$

In the formula,

ζ ——flow resistance coefficient

Δp ——pressure loss, Pa

ρ ——media density, kg/m^3

v ——the average flow, m/s

Lighthill Acoustic Theory

The proposed Lighthill sound theory underpins stream noise research and development. The proposed Lighthill theory of acoustic analogy is based on the assumption that a finite region of turbulent motion V is contained in an infinitely large homogeneous, static acoustic medium. This means that outside the region of turbulent motion V is largely unaffected by the turbulent motion region V, and that density fluctuations in the flow field are similar to acoustic waves. Lighthill suggested that the fluid's continuity equation and momentum equation serve as the foundation for the acoustic analogy theory's derivation. By collating the simplified continuity equation and momentum equation of the fluid, the homogeneous acoustic fluctuation equation in the fluid far from the turbulent region is obtained, as shown in Eq. (7) (Bravo *et al.* 2016; Lighthill 1952):

$$\frac{1}{c_0} \frac{\partial \rho'}{\partial t^2} - \nabla^2 \rho' = 0 \qquad (7)$$

where, $\rho' = \rho - \rho_0$, ρ and ρ' are the fluid densities when disturbed and undisturbed, respectively. C_0 is the value of the sound velocity under equal first conditions.

The continuity equation and momentum equation under the basic assumptions can be written as shown in Eq. (8) and Eq. (9). (Tang *et al.* 2017)

$$\frac{\partial \rho}{\partial t} + \frac{\partial \rho u_i}{\partial x_i} = 0 \qquad (8)$$

$$\frac{\partial \rho u_i}{\partial t} + \frac{\partial \rho u_i u_j}{\partial x_i} = -\frac{\partial p}{\partial x_i} + \frac{\partial \tau_{ij}}{\partial x_j} \qquad (9)$$

In Eq. (9), $\tau_{ij} = \mu \left(\frac{\partial u_i}{\partial x_j} + \frac{\partial u_j}{\partial x_i} - \frac{2}{3} \delta_{ij} \frac{\partial u_k}{\partial x_k} \right)$ represents the viscous part of the Reynolds stress tensor. Eq. (10) can be obtained by differentiating Eq. (8) with respect to *t*. Then, taking the scatter of Eq. (10) yields Eq. (11). (Wu *et al.* 2021)

$$\frac{\partial^2 \rho}{\partial t^2} + \frac{\partial^2 (\rho u_i)}{\partial x_i \partial t} = 0 \qquad (10)$$

$$\frac{\partial^2 (\rho u_i)}{\partial x_i \partial t} + \frac{\partial^2 \rho u_i u_j}{\partial x_i \partial x_j} = -\frac{\partial^2 p}{\partial x_i^2} + \frac{\partial^2 \tau_{ij}}{\partial x_i \partial x_j} \qquad (11)$$

Subtracting momentum Eq. (9) from Eq. (11), we can obtain Eq. (12):

$$\frac{\partial^2 \rho}{\partial t^2} - \frac{\partial p}{\partial x_i^2} = \frac{\partial^2}{\partial x_i \partial x_j} \left(\rho u_i u_j - \tau_{ij} \right) \qquad (12)$$

Subtracting $c_0^2 \nabla^2 \rho$ from both sides simultaneously yields Eq. (13):

$$\frac{\partial^2 \rho}{\partial t^2} - c_0^2 \nabla^2 \rho = \frac{\partial^2}{\partial x_i \partial x_j} \big[\rho u_i u_j - \tau_{ij} + \\ \delta_{ij}(p - c_0^2 \rho) \big] \qquad (13)$$

For the far-field region unaffected by the turbulent region, the derivative is naturally zero since ρ_0 is constant. Let $T_{ij} = \rho u_i u_j - \tau_{ij} + \delta_{ij}(p - c_0^2 \rho)$. By changing the formula above into Eq. (13), the equation of density fluctuation can be obtained as shown in Eq. (14). The formula is the famous Lighthill equation (Wright *et al.* 2015).

$$\frac{\partial^2 \rho'}{\partial t^2} - c_0^2 \nabla^2 \rho' = \frac{\partial T_{ij}}{\partial x_i \partial x_j} \qquad (14)$$

The generation and propagation of sound are calculated separately by the Lighthill acoustic analogy method. The acoustic calculation model based on steady or transient flow field calculations built in CFD software can convert the flow field data into a sound source to calculate the sound field, so the requirements of calculation amount and calculation format are low (Yao *et al.* 2022). The acoustic analogy method has already possessed engineering application value. It has been used in a variety of fields, including the far-field aerodynamic noise of high-speed vehicles and the far-field aerodynamic noise of high-speed trains (Du *et al.* 2022; Narayanan *et al.* 2021)

3.2 Three-dimensional Modeling and Meshing

The calculation models of the flow field and sound field are established by Creo 3-D modeling software. This paper is primarily concerned with the muffler's external sound field characteristics. Therefore, when building the sound field calculation model, water is added around the muffler. The ANSYS-ICEM software is used to mesh the muffler 3D model. The flow field and sound field meshes are meshed with an unstructured tetrahedral mesh to account for the irregularity of the muffler structure. According to the sound field grid requirements, the maximum size of the sound field grid must be less than one-sixth the length of the maximum sound wave. To ensure the accuracy of the calculation, five different sets of grids are listed to verify the grid independence with the pressure difference as the measurement standard. The results of grid independence verification are shown in Fig. 5. The final decision is to set the grid cell size to 4 mm, the location of the circular hole is locally encrypted, and the number of grids is 244 million. The flow and sound fields are computed using the same grid set. The flow field computing domain grid and sound field computing domain grid are shown in Fig. 6.

3.3 Flow Field and Sound Field Numerical Calculation Settings

The muffler flow field calculation is based on the ANSYS-CFX platform. The steady-state calculation
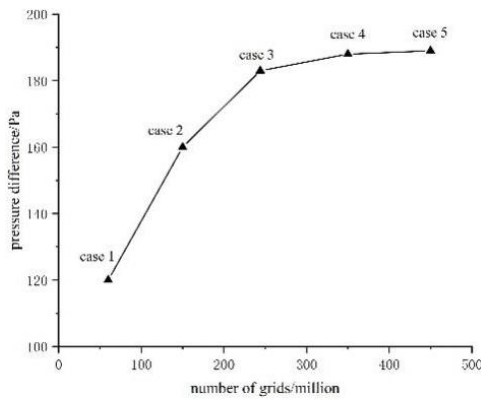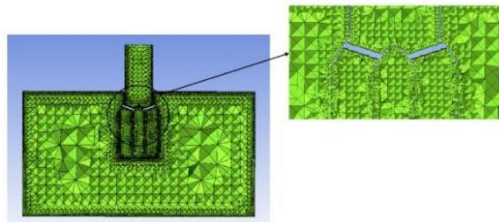
Fig. 5. Grid Irrelevance Verification.
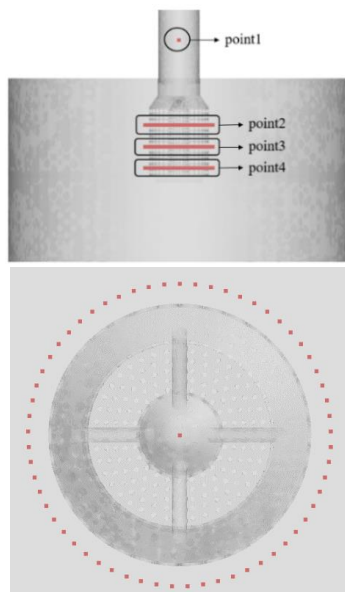

Fig. 6. Muffler grid.

Fig. 7. Location of sound field monitoring points.

is the first step in the numerical simulation of the muffler flow field. Unsteady-state computations are done after acquiring the steady-state flow field. $k - \varepsilon$ turbulence models are used for both steady and unsteady calculations. The effect of temperature change on hydrodynamic noise is ignored. The inlet flow and outlet pressure serve as the muffler's inlet and outlet boundary conditions. The inlet meets three flow conditions of 200 m³/h, 400 m³/h and 600 m³/h. The pressure at the outlet is set to 1 MPa. The transient calculation time step is set to 0.0003s, and the overall time step is set to 0.3 s. The wall surface

roughness is set to 0.03 mm. It is utilized for hydrodynamic noise calculation and analysis by extracting the time domain pressure pulsation sound source information of the muffler in the flow field.

The acoustic software ACTRAN is used to calculate the sound field. The sound field outside the muffler is calculated using time domain information from the flow field. The ACTRAN-ICFD module can use the Fourier transform to obtain the sound source term in the frequency domain. The hydrodynamic noise calculation frequency of the muffler is set to 0-1000 Hz. The full absorption surface is the boundary condition for the muffler's inlet and outlet. The remainder of the wall surface is configured to be completely reflective. The locations of the monitoring points are shown in Fig. 7. To obtain the accurate noise condition of the muffler outlet, the surrounding monitoring points are set at the outlet. There are 61 points in the surrounding monitoring points, and these points are distributed around the center along the circumference at equal angles. The diameter of the distribution circle of monitoring points is set to 0.4 m.

## 4. ANALYSIS OF SIMULATION RESULTS

4.1 Analysis of Flow Field Results

The muffler's pressure change primarily includes the friction pressure change caused by friction between the muffler's inner channel wall surface and the fluid. The change in fluid flow state caused by the change in the local structure in the muffler causes the local pressure difference. Generally, the local loss occupies the main position. Table. 1. shows the pressure difference and resistance coefficient under different flow conditions. According to the results, the resistance coefficient of this muffler is approximately 2.09.

Table 1 Pressure difference and flow resistance coefficient of the muffler

| Working condition (m³/h)	200	400	600
Pressure difference (Pa)	23.9	85.9	182.8
Flow resistance coefficient	2.27	2.06	1.95

Figure 8 shows the pressure distribution clouds for 200 m³/h, 400 m³/h and 600 m³/h flow conditions. Under different flow rates, the pressure distribution at each place of this muffler is uniform, and the flow pattern is stable. The pressure at the inlet pipe is slightly less compared to the pressure at the outlet. The overall pressure in the pool does not vary much and the pressure values are stable within a range. The momentum transfer of the jet (divided by the area) causes the pressure in the pool to increase. The flow velocity is very small during the actual flow, the pressure distribution in the pool is uniform, and the flow at the bottom of the muffler is more violent. The flow velocity at the bottom of the pool is slightly faster compared to the surface of the pool, while the flow at the surface of the pool is almost stationary,
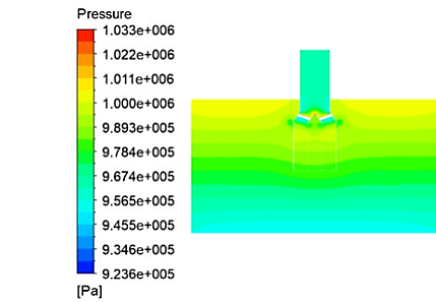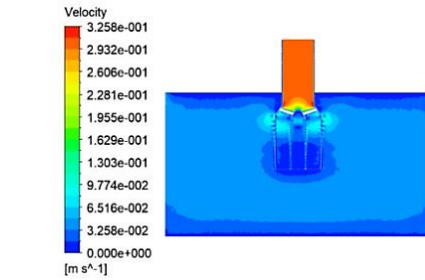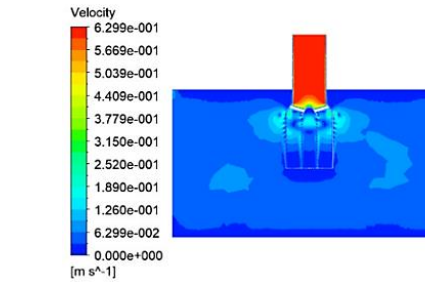
(1) 200 m³/h
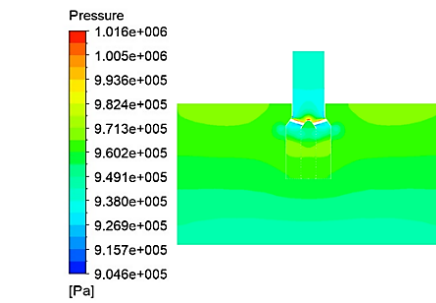
(2) 400 m³/h
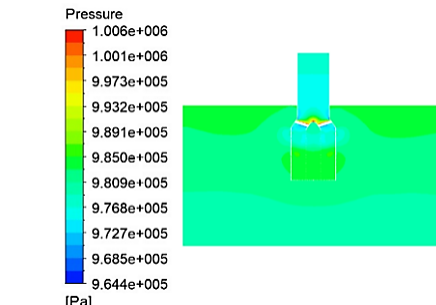
(3) 600 m³/h

Fig. 8. Pressure distribution clouds under different flow conditions.

(1) 200 m³/h

(2) 400 m³/h

(3) 600 m³/h

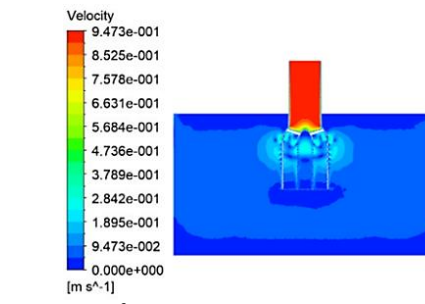**Fig. 9. Velocity distribution clouds under different flow conditions.**

resulting in the phenomenon that the pressure at the bottom of the pool is slightly less than the surface of the pool. Fig. 9 shows the velocity distribution clouds under various working conditions. As can be seen in the diagram: the flow velocity is faster at the inlet of the muffler, and gradually decreases after the diversion of the water guide cone. Due to the increase in the outlet area, the flow velocity of the muffler outlet water location is small compared with that of the inlet, and the flow velocity reaches the lowest value. Fig. 10 shows the vorticity map under different flow conditions. In the figure, it can be seen that a large number of high-speed vortices at the inlet of the muffler pass through the diversion of the water guide cone, and the flow velocity and vorticity gradually decrease. Especially at the middle and lower ends of the muffler outlet, very few vortices enter the pool. Therefore, the pressure change of the pool is very small, and the flow state is relatively stable. Based on the flow field's numerical calculation results, the muffler structure stabilizes the flow. After the transition of the fluid in the pipe through the muffler, the pressure fluctuation and flow velocity when flowing to the pool are reduced. The main source of hydrodynamic noise is caused by

fluid turbulence. The muffler of this structure is installed at the outlet of the pump piping system, which has a certain contribution to noise reduction. Simultaneously, the flow field numerical simulation results lay the groundwork for calculating the external noise of the muffler below.

4.2 External Sound Field Results Analysis

Based on the flow field results analysis, it is concluded that the muffler has a certain muffling capacity. To further investigate the muffling performance of this muffler, the external sound field of the muffler is studied. Fig. 11 to Fig. 13 show the frequency domain of the sound pressure level (SPL) at the inlet and outlet monitoring points for each flow condition. The results of the numerical simulation are compared to the filtered experimental data, and both have similar SPL trends. As a result, the numerical simulation method's validity is confirmed. The numerical simulation results are credible. The frequency domain distribution of the selected monitoring points in each group is shown in the figure to be similar under different working conditions. The main frequency is mainly around at 13.32 Hz, and the peak SPL is concentrated at this frequency. Under the same flow conditions, the same location monitoring point with increased frequency.
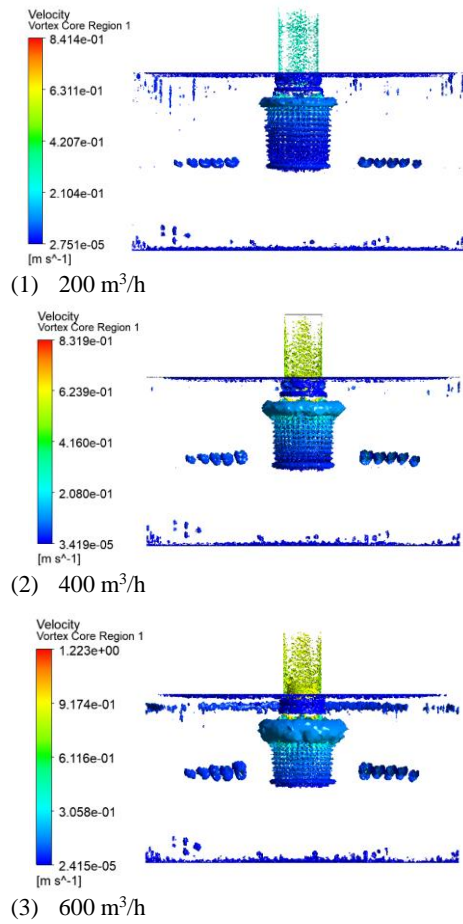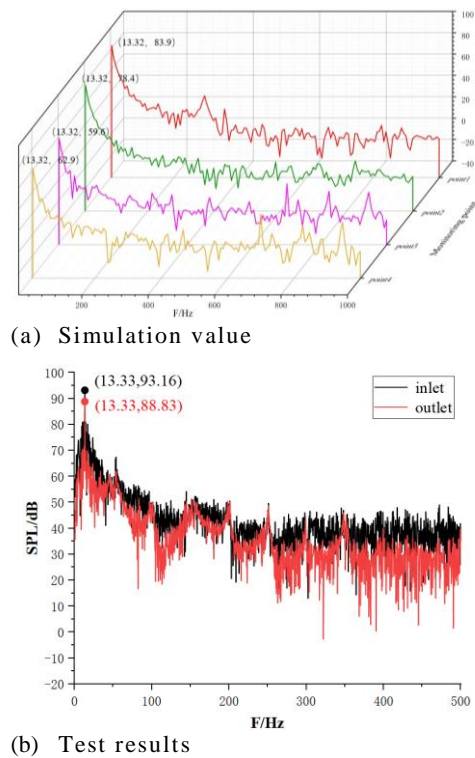
(1) 200 m³/h

(2) 400 m³/h

(3) 600 m³/h

Fig. 10. Vorticity maps.

(a) Simulation value

（b）Test results

Fig. 12. Sound pressure level frequency domain diagram (400 m³/h).

(a) Simulation value

(b) Test results

Fig. 11. Sound pressure level frequency domain diagram (200 m³/h).

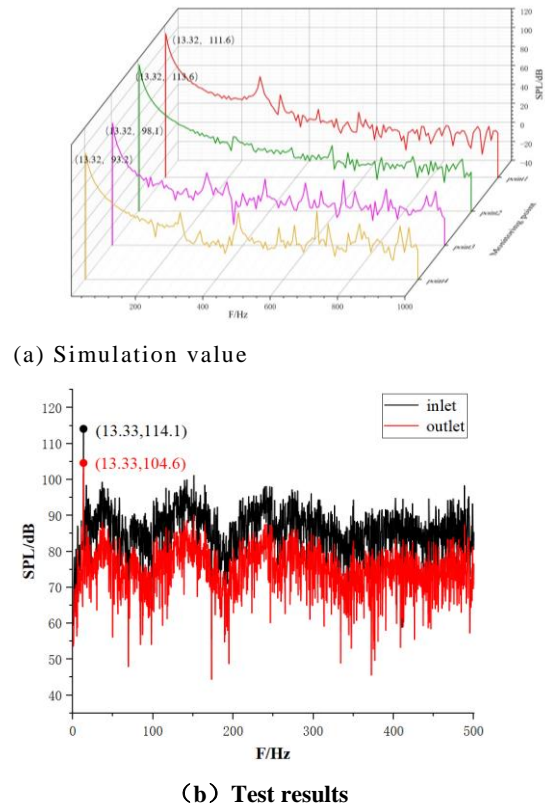(a) Simulation value

（b）Test results

Fig. 13. Sound pressure level frequency domain diagram (600 m³/h).

Table 2 Overall sound pressure levels comparison

Traffic conditions	Monitor	overall sound pressure level (OASPL)
200m³/h	Point1	89.7 dB
	Point2	84.3 dB
	Point3	65.6 dB
	Point4	66.4 dB
400m³/h	Point1	112.3 dB
	Point2	105.2 dB
	Point3	87.7 dB
	Point4	85.5 dB
600m³/h	Point1	117.5 dB
	Point2	120.5 dB
	Point3	101.4 dB
	Point4	98.9 dB

The intensity of sound pressure steadily diminishes and eventually fluctuates within a narrow range. The noise increases with increasing of flow rate for different flow conditions. When the pump piping system is running, the inlet of the muffler (monitoring point 1) has a high noise level. After the muffler's shunt muffling, the noise is reduced more obviously.

Table. 2 shows overall sound pressure level (OASPL) at various monitoring point positions. The muffler inlet has a OASPL of 89.7 dB, 112.3 dB and 117.5 dB for 200 m³/h, 400 m³/h and 600 m³/h flow rates, respectively. As the position of the monitoring point moves toward the muffler outlet, the OASPL gradually decreases. The monitoring point 2 position is in a transitional state. When it reaches the positions of monitoring points 3 and 4, the noise has a significant decrease. The OASPL at monitoring point 4 are 66.4 dB, 85.5 dB and 98.9 dB. Comparing muffler inlet monitoring point 1 with outlet monitoring point 4, the OASPL decreases by approximately 20 dB. This result shows that this muffler structure has good muffling performance when applied to a pump piping system. It can effectively avoid the exit noise transmission and the reflection of the pool wall noise

Figure 14 shows directivity curve of the SPL of the sound field at the muffler outlet. It can be seen in the figure that the radiation directivity of the muffler outlet sound field is closest to that of the quadrupole sound source. It has the characteristics of a quadrupole sound source. A quadrupole source is a medium in which no mass or heat is injected and no obstacle exists, but is formed only by acoustic waves radiated by viscous stress. It is considered a stress sound source. A quadrupole can be seen as a pair of dipoles of opposite polarity, pointing in a "four-leaf rose shape". The quadrupole sound source is the main contributor in this pipeline. As the flow rate increases, the characteristics of the quadrupole sound source become increasingly obvious at the field points near 67°, 157°, 247° and 337°. This provides guidance for research on noise reduction. Fig. 15. shows the distribution cloud of the SPL at the characteristic frequency. As illustrated in the figure, the muffler's higher SPL is primarily concentrated at the inlet end. When the noise is
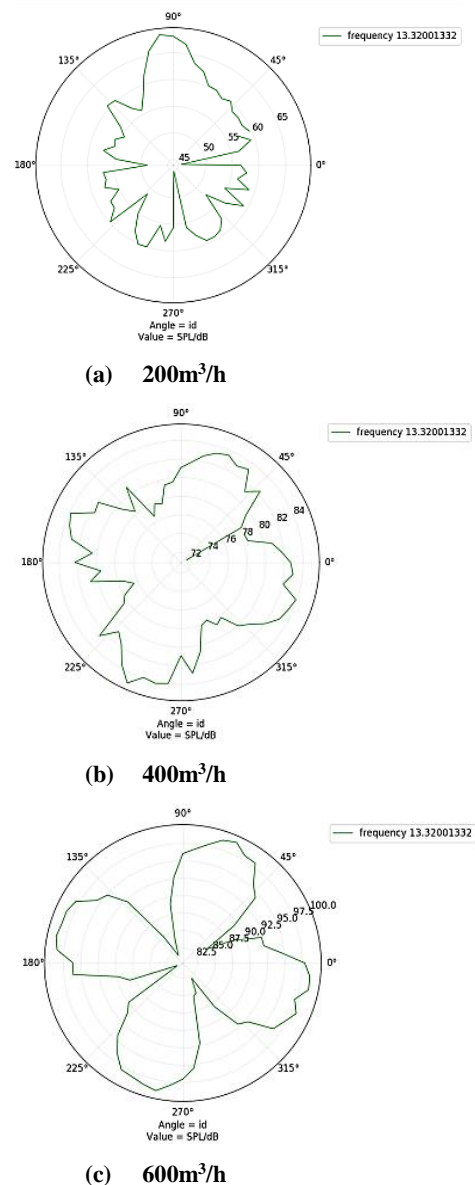

(a)   200m³/h

(b)   400m³/h

(c)   600m³/h

Fig. 14. Sound pressure level directivity curve.

radiated into the pool through the muffler, the noise is obviously reduced. In conjunction with the flow field analysis, the reason for this phenomenon is the

main vortices are gathered at the inlet of the muffler, and there are very few vortices in the pool. The vortex velocity at the inlet of the muffler is larger than that at the outlet. Because of the presence of numerous high-speed vortices in the inlet pipe, fluid flow is unstable. The muffler's SPL is higher at the inlet. After the diversion of water guide cone and the increase of overflow area, the number of vortices in each outlet hole is reduced and the vortex velocity is lowered. The SPL at the outlet pool of the muffler is reduced to a large extent, which plays a role in muffling the sound.
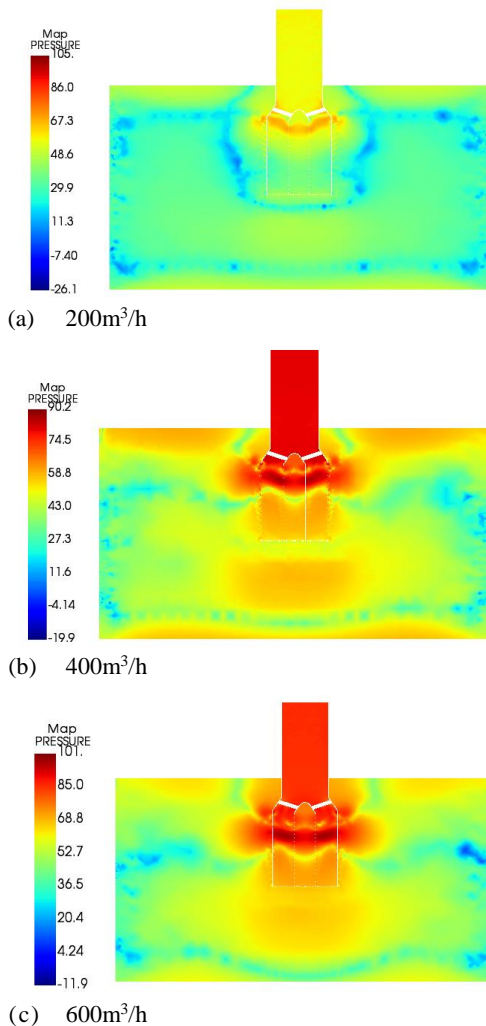
(a)   200m³/h

(b)   400m³/h

(c)   600m³/h

Fig. 15. Sound pressure level distribution cloud at the main frequency.

5.   CONCLUSION

A new type of structured muffler is proposed in this paper. This muffler can be widely used in pump piping systems. The diversion effect of the water guide cone reduces the impact noise of the medium in the pipe. And the flow pattern has been enhanced. The method of opening holes on the muffler wall and extending the flow path is adopted to increase the overflow area, which reduces the fluid flow velocity in the pipeline and the number of vortices. Compared with other mufflers, the muffler proposed in this paper is based on the optimization of fluid flow characteristics, thus optimizing the hydrodynamic noise and finally achieving the purpose of reducing the outlet noise of the pipeline system. This muffler can effectively muffle low frequency, medium frequency and high frequency noise at the same time, breaking the limitation that some mufflers can only strongly muffle specific frequencies. Furthermore, the muffler proposed in this paper is simple to process and easy to disassemble and install. The conclusions about this muffler obtained in this paper are as follows:

(1)   Under the three flow conditions, the characteristic peak value of the muffler noise is approximately 13.32 Hz. The general trend is that as frequency increases, noise gradually decreases and eventually fluctuates within a numerical range.

(2)   This muffler has a good silencing effect. By comparing the inlet and outlet of the muffler, as the pressure decreases, the noise gradually decreases by approximately 20 dB. The flow resistance coefficient of the muffler is approximately 2.09 after calculation. This paper's research content can be used to design mufflers for pump pipeline systems. It has the advantages of environmental protection, convenient fabrication and improving ship stealth performance.

(3)   The radiation directivity of the muffler outlet sound field is the closest to that of the quadrupole sound source. It has the characteristics of a quadrupole sound source. With increasing flow rate, the characteristics of the quadrupole sound source become increasingly obvious. Quaternary sources become the primary sources of noise.

REFERENCES

Bravo, T., C. Maury and C. Pinhède (2016). Optimisation of micro-perforated cylindrical silencers in linear and nonlinear regimes. *Journal of Sound & Vibration* 363, 359-579.

Chen, Z. C., C. M. Mark and X. Wang (2017). Noise attenuation performance improvement by adding Helmholtz resonators on the periodic ducted Helmholtz resonator system. *Applied Acoustic* 122, 8-15.

Dai, C., Y. Zhang and Q. Pan (2021). Study on

Vibration Characteristics of Marine Centrifugal Pump Unit Excited by Different Excitation Sources. *Journal of Marine Science and Engineering* 9(3), 274.

Du, L. M., C. J. Bian and P. Zhang (2022). Aerodynamic Response Analysis of High-Speed Trains Passing through High Platforms under Crosswind. *Journal of Applied Fluid Mechanics* 15(5), 1525-1543.

Gai, X. L., T. Xing, Z. X. Kang, X. H. Li, B. Zhang, Z. N. Cai, F. Wang and X. W. Guan (2020). Study on sound insulation performance of the periodic arrangement expansion chambers structure with built-in micro-perforated panel. *Applied Acoustics* 161, 107187.

Gu, C. Z., Y. Liu, R. R. Luo and X. J. Qiu (2018). Study on vibration causes and in-situ suppression strategy of ship engine room pipeline. *Mechanical Engineer* 11, 135-137, 141.

Hou, J. X., H. C. Zhu and S. W. Yuan (2020). Low-frequency and wide-band noise elimination characteristics of elastic back cavity plate muffler. *Vibration and Shock* 39(20), 251-257, 273.

Lee, J. W (2015). Optimal topology of reactive muffler achieving target transmission loss values: Design and experiment. *Applied Acoustics London* 88, 104-133.

Li, Y. F., H. J. Shen, L. K. Zhang, Y. S. Su and D. L. Yu (2016). Control of low-frequency noise for piping systems via the design of coupled band gap of acoustic metamaterials. *Physics Letters A*, 2322-2328.

Liang, X. D. (2010). Influence of pipeline vibration and noise on overall acoustic stealth characteristics of ships. *Noise and Vibration Control* 6, 127-128, 135.

Lighthill, M. J. (1954). Turbulence as a source of sound. *Proc.r.soc.a* 222(1148), 1-32.

Lighthill, M. J. (1952). On Sound Generated Aerodynamically. I. General Theory. Proceedings of the Royal Society of London. *Series A, Mathematical and Physical Sciences* 211(1107), 564-587.

Liu, F. S., H. Wang and Q. Z. Zhang (2020). Comparative Experimental study on flow Resistance characteristics of Tri-eccentric Butterfly Valve. *Fluid Machinery* 48(3), 12-16.

Liu, H. L., J. W. Lin, R. N. Hua and L. Dong (2022). Structural optimization of muffler for marine pumping system based on numerical calculation. *Journal of Marine Science and Engineering* 10(7), 937.

Liu, H. L., J. Ding and Y. Wang (2013). Numerical simulation of hydrodynamic noise of centrifugal pump based on large eddy simulation. *Journal of Mechanical Engineering* 18, 177-183.

Lyu, C. M., H. F. Lyu and X. G. Zhang (2020). Optimization design of Helmholtz resonance muffler. *Acoustic Technology* 39(2), 230-34.

Narayanan, S. Syam and R. Asad Ahmed (2021). Effect of Fluid-Structure Interaction on Noise Generation in MAV with Fixed and Flapping Membrane Wing. *Journal of Applied Fluid Mechanics* 14(6), 1817-1826.

Shao, H., H. He, Y. Chen, X. Tan and G. Chen (2020). A tunable metamaterial muffler with a membrane structure based on Helmholtz cavities. *Applied Acoustics* 157, 107022.

Tang, C. D., Z. P. Wang and Y. Z. Sima (2017). Systematical research on the aerodynamic noise of the high-lift airfoil based on FW-H method. *Journal of Vibroengineering* 19(6), 4783-4789.

Wu, X. B., J. F. Wang and X. Y. Zhang (2021). Water jet noise analysis of different nozzle structures. *Journal of Harbin Engineering University* 42(8), 1162-1166.

Wright, M. C. M. and C. L. Morfey (2015). On the extrapolation of acoustic waves from flow simulations with vortical out flow. *International Journal of Aeroacoustics* 14(1-2), 217-227.

Xia, J., Y. Y. Zhang and Q. B. Pan (2017). Design and experimental study of pipeline low noise drainage Device. *Ship Science and Technology* 39(1), 90-5.

Xiang, L., S. Zuo, X. Wu and J. Liu (2017). Study of multi-chamber micro-perforated muffler with adjustable transmission loss. *Applied Acoustics* 122(JUL.), 35-40.

Yao, Y., Z. Sun, G. Li, P. Prapamonthon, G. Cheng and G. Yang (2022). Numerical Investigation on Aerodynamic Drag and Noise of Pantographs with Modified Structures. *Journal of Applied Fluid Mechanics* 15(2), 617-631.

Zhang, Z., D. Yu, J. Liu, B. Hu and J. Wen (2021). Transmission and bandgap characteristics of a duct mounted with multiple hybrid Helmholtz resonators. *Applied Acoustics* 183, 108266.

Zhang, Z. H., J. Chen and S. Z. Wang (2006). Numerical simulation of internal flow field of muffler. *Vibration and Shock* 25(6), 21-24.

Zhou, Y., H. M. Luo and H. T. Fan (2018). Theoretical calculation and structural optimization of transmission loss of multi-cavity perforated muffler. *Manufacturing Automation* 40(9), 102-106.

Zuo, S. G., G. Long and X. D. Wu (2014). Influence of partition on acoustic characteristics of automobile micro-perforated pipe muffler. *Journal of Agricultural Engineering* 30(11), 53-59.